

Generalized MIMO Transmit Preprocessing Using Pilot Symbol Assisted Rateless Codes

Nicholas Bonello, Du Yang, Sheng Chen, and Lajos Hanzo

Abstract—In this paper, we propose a generalized multiple-input multiple-output (MIMO) transmit preprocessing system, where both the channel coding and the linear MIMO transmit precoding components exploit the knowledge of the channel. This was achieved by exploiting the inherently flexible nature of a specific family of rateless codes that are capable of modifying their code-rate as well as their degree distribution based on the channel state information (CSI), in an attempt to adapt to the time-varying nature of the channel. Moreover, we also propose a novel technique, hereby referred to as pilot symbol assisted rateless (PSAR) coding, where a predetermined fraction of binary pilot symbols is interspersed with the channel-coded bits at the channel coding stage, instead of multiplexing the pilots with the data symbols at the modulation stage, as in classic pilot symbol assisted modulation (PSAM). We will subsequently demonstrate that the PSAR code-aided transmit preprocessing scheme succeeds in gaining more beneficial knowledge from the inserted pilots, because the pilot bits are not only useful for estimating the channel at the receiver, but they are also beneficial in terms of significantly reducing the computational complexity of the rateless channel decoder. Our results suggest that more than a 30% reduction in the decoder's computational complexity can be attained by the proposed system, when compared to a corresponding benchmark scheme having the same pilot overhead but using the PSAM technique.

Index Terms—Generalized transmit preprocessing, MIMO, pilot symbol assisted rateless codes, rateless codes, complexity reduction, pilot symbol assisted modulation.

I. INTRODUCTION

ONE of the most significant technological breakthroughs of contemporary wireless communications is constituted by multiple-input multiple-output (MIMO) transceivers, which provide an elegant solution for further extending the channel's capacity limits [1] and/or for enhancing the link's reliability [2]. More pronounced efficiency gains can be expected, if both the transmitter and receiver are capable of exploiting channel state information (CSI).

In such systems, the CSI extracted at the receiver (CSIR) is typically obtained by estimating the unknown channel parameters based on known pilot bits. This CSI may also be fed back to the transmitter using a feedback channel. The resultant CSI at the transmitter (CSIT) may be exploited by a technique that is commonly referred to as transmit preprocessing [3],

Manuscript received February 23, 2009; revised July 14, 2009 and August 31, 2009; accepted October 20, 2009. The associate editor coordinating the review of this paper and approving it for publication was A. Grant.

The authors are with the School of ECS, University of Southampton, SO17 1BJ, United Kingdom (e-mail: {nb06r, dy05r, sqc, lh}@ecs.soton.ac.uk).

The financial support of both the EPSRC U.K., and that of the EU under the auspices of the Optimix project, is gratefully acknowledged.

Digital Object Identifier 10.1109/TWC.2010.02.090276

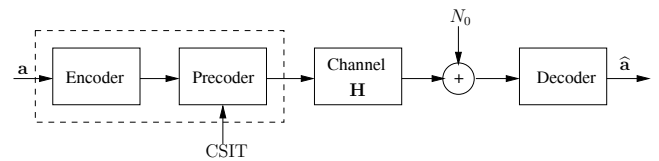


Fig. 1. The transmit preprocessing scheme proposed by Vu and Paulraj in [3].

as exemplified in Figure 1. This configuration consists of two separate components; a predetermined (i.e. fixed-rate), CSIT-independent channel coding scheme amalgamated with a linear CSIT-dependent MIMO transmit precoder. In this paper we are advocating a solution, where both the channel coding as well as the linear MIMO transmit precoder components exploit the knowledge of CSIT. We argue that since the scheme of [3], which is illustrated in Figure 1, already received CSIT with the aid of a readily available feedback channel from the receiver, then providing CSIT information not only for the MIMO precoder but also for the channel encoder does not impose substantial complications. In doing so, we are adopting a wider perspective by amalgamating the two CSI-assisted components, namely, the channel encoder and the MIMO linear precoder, into a more generalized transmit preprocessing block.

The first modification that has to be carried out for the system of Figure 1 [3], is that the channel code to be employed can now no longer have predetermined constraints, such as that of having a fixed-rate and a rigid construction, but has to additionally rely on online processing techniques for exploiting the available CSIT, in a similar manner to that of the linear MIMO transmit precoder. A channel code that does not have a fixed-rate is commonly referred to as being a *rateless code* [4], [5]. Alternatively, a rateless code can be interpreted as an inherently flexible channel code that subsumes a potentially infinite number of fixed-rate codes. The second modification that we impose is actually related to the degree distribution employed by the rateless codes. In the available literature [5]–[8], rateless codes are frequently employed in situations, where the channel statistics are unknown to the transmitter and hence the degree distribution of rateless codes is fixed; i.e. the degree distribution used for coining the specific random degree for each transmitted bit is time-invariant and thus channel-independent. Such rateless codes can only control the total the number of bits transmitted, i.e. the code-rate, in order to cater for the variations of the channel conditions encountered. In [9], we have studied the degree distribution of a rateless code, analyzed the optimum distribution across a diverse range of channel signal-to-noise ratio (SNRs) and demonstrated that

there are substantial differences between these distributions. Consequently, we reaffirmed the arguments presented in [10] that rateless codes having a fixed degree distribution are sub-optimal in the sense that they cannot realize codes that operate near to capacity at all possible rates. However, in the specific scenario we are considering here, the rateless encoder is armed with side information and therefore it is capable of calculating in a near-realtime online manner, the specific degree distribution that results in a performance which is arbitrarily close to capacity.

Another contribution of this paper is related to the channel estimation to be used at the receiver for determining the CSIR. There are mainly two approaches that are frequently employed to estimate the channel; namely that of either estimating the channel blindly or using reference/pilot symbols. For all intents and purposes of this paper, the downlink (DL) receiver of the mobile station (MS) estimates the channel's amplitude and phase using known pilots and then conveys this CSI estimate back to the DL transmitter of the base station (BS). However, instead of inserting pilots at the modulation stage as in classic PSAM, we propose a novel rateless code, termed as the pilot symbol assisted rateless (PSAR) code, which appropriately intersperses a predetermined fraction of pilot bits with the codeword bits. The motivation behind using PSAR codes is that of gleaning more information from the pilot overhead "investment", than just simply the capability of channel estimation such as in the PSAM technique.

Against this background, the novelty and rationale of this paper can be summarized as follows:

- 1) We propose a generalized transmit preprocessing aided closed-loop downlink MIMO system, in which both the channel coding components and the linear transmit precoder exploit the knowledge of the CSI. In order to achieve this aim we have embedded, for the first time, a rateless code in our transmit preprocessing scheme, in order to attain a near-capacity performance across a wide range of channel SNRs.
- 2) In contrast to conventional rateless codes, which use a fixed degree distribution, the proposed rateless codes are capable of calculating the required degree distributions prior to transmission based on the available CSIT. In doing so, we amalgamate the rateless encoder and the linear MIMO precoder into a generalized transmit preprocessing scheme.
- 3) Furthermore, we propose a novel technique, hereby referred to as PSAR coding, where a predetermined fraction of pilot bits is appropriately interspersed with the original information bits at the channel coding stage, instead of multiplexing pilots at the modulation stage, as in classic PSAM. We will subsequently demonstrate that the PSAR code-aided transmit preprocessing scheme succeeds in gleaning more information from the inserted pilots than the classic PSAM technique, because the pilot bits are not only useful for sounding the channel at the receiver but also beneficial for significantly reducing the computational complexity of the rateless channel decoder.

The rest of this paper is organized as follows. Section II and III contain the description of the channel model and the

system model, respectively. A detailed graph-based analysis of PSAR codes is offered in Section IV. The extrinsic information transfer (EXIT) chart functions of PSAR codes were then derived in Section V. In Section VI, we have detailed the specific algorithm that was employed for the 'on-the-fly' calculation of the PSAR code's degree distributions based on the available CSIT. Our simulation results are then presented in Section VII. Finally, Section VIII provides a brief summary of the paper, followed by our final conclusions.

II. CHANNEL MODEL

We consider a single-user MIMO system employing two transmit and two receive antennas. The canonical continuous-time complex baseband-equivalent MIMO channel model used is given by $\mathbf{y}(t) = \mathbf{H}(t)\mathbf{x}(t) + \mathbf{n}(t)$, where $\mathbf{x}(t)$, $\mathbf{y}(t) \in \mathbb{C}$ are vectors corresponding to the transmitted and received signals of the respective antennas. The time-variant MIMO channel matrix $\mathbf{H}(t)$ contains elements corresponding to the channel gains of a Rayleigh-fading process generated according to a complex circularly symmetric Gaussian distribution and with an autocorrelation function $r_{aa}(\tau)$ formulated by $r_{aa}(\tau) = J_0(2\pi\bar{f}_m\tau)$, where τ represents the correlation lag, $J_0(\cdot)$ represents the zero-order Bessel function of the first kind and \bar{f}_m is the normalized Doppler frequency. The complex additive white Gaussian noise (AWGN) is represented by the vector $\mathbf{n}(t) \sim \mathcal{CN}(0, N_0)$, where N_0 denotes the two-dimensional noise variance.

The near-instantaneous SNR encountered at the receiver antenna i , $\bar{\psi}_i$, and associated with a particular channel realization $\mathbf{h}_i(t) = [h_{i,1} \ h_{i,2}]$ is then given by $\bar{\psi}_i := E_s |\mathbf{h}_i(t)|^2 / N_0$, where E_s and $|\mathbf{H}(t)|^2$ represent the constant energy-per-symbol at a specific antenna and the fading power coefficients, respectively. The average SNR at the receiver is then given by $\psi_{i,\text{avg}} := [E_s \mathcal{E}(|\mathbf{h}_i(t)|^2)] / N_0$, where $\mathcal{E}(\cdot)$ denotes the expectation operator. Since the statistical distribution of the channel realizations between any two pair of transmit and receive antennas is identical, then the average SNR at each antenna is also identical. Consequently, we will simply use the MIMO system's SNR, denoted here by ψ_{avg} .

III. SYSTEM MODEL

Figure 2 illustrates a top-level schematic of the proposed system model. For the sake of simplifying our analysis, we will refer to the two CSI-assisted components in the system as the inner and outer closed-loops. The outer closed-loop system consists of a reconfigurable rateless code [9]. However, in contrast to the work presented in [9], we enhance the achievable performance by appropriately embedding pilots symbols into the generated codeword. The inner closed-loop system is then constituted by a single-user MIMO transmit eigen-beamforming scheme. These two components of Figure 2 are separated by a pilot position interleaver and by an Alamouti space-time block code (STBC) [11]. Furthermore, we assume an error- and delay-free feedback channel having infinite accuracy.

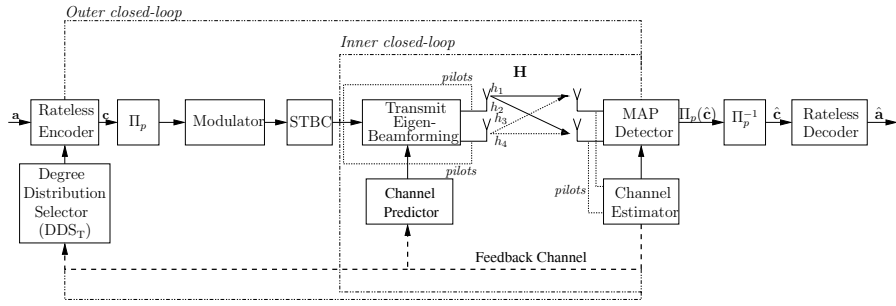


Fig. 2. The generic system model, having two components of the system that are exploiting CSI feedback in the inner and outer closed-loops.

A. Outer Closed-Loop: Encoder for Pilot Symbol Assisted Rateless Codes

For every information bit sequence to be encoded at a specific transmission instant ι , the CSI received via the feedback channel is exploited by what we refer to as the degree distribution selector¹ (DDS) of Figure 2 in order to calculate the required coding rate R_ι as well as the corresponding irregular degree (or check node) distribution $\delta_\iota(x)$. The latter can be conveniently represented by means of a polynomial distribution defined by:

$$\begin{aligned} \delta_\iota(x) &:= \sum_{\forall d_c \in \mathbf{d}^\iota} \delta_{d_c} x^{d_c-1} \\ &= \delta_1 + \delta_2 x + \dots + \delta_{d_c} x^{d_c-1} + \dots + \delta_{D_c} x^{D_c-1}, \end{aligned} \quad (1)$$

where the positive coefficients δ_{d_c} , $d_c \in \mathbf{d}^\iota$ denote the particular fraction of intermediate bits (or check nodes) of degree d_c and $D_c = \max(\mathbf{d}^\iota)$ is the maximal check (left) degree. The vector \mathbf{d}^ι contains the range of (check) degree values of the degree distribution. In contrast to [9], there is now two different categories of degree-one bits and as a result, the fraction δ_1 of (1) can be rewritten as $\delta_1 = \delta_1^p + \delta_1^i$, where δ_1^p and δ_1^i denote the fraction of degree-one nodes corresponding to pilot bits and to information bits, respectively. The rateless encoder of Figure 2 maps a K -bit (input) information sequence represented by $\mathbf{a} = [a_1, a_2, \dots, a_K]$ into a $(K' R_\iota^{-1})$ -bit output sequence \mathbf{c} by performing the steps succinctly described below:

- 1) (*Modified input bit sequence*) Attach a predetermined pilot-bit sequence $\mathbf{p} = [p_1, p_2, \dots, p_{K_p}]$, to the beginning of the K -bit input stream \mathbf{a} , so that the modified K' -bit input sequence becomes equal to $\mathbf{a}' = [\mathbf{p} \mathbf{a}]$;
- 2) (*Degree selection*) Randomly choose a degree d_c from a degree distribution $\delta_\iota(x) - \delta_1^p$ calculated by the degree distribution selector based upon the received CSI;
- 3) (*Input bit/s selection*) Randomly choose the previously selected d_c number of bits from \mathbf{a}' having the least number of connections (selections) up to the current transmission instant;
- 4) (*Intermediate bit calculation*) The value of the each of the intermediate (check) bit $b_i \in \mathbf{b}$ is calculated by means of combining the d_c input bits selected during the previous step using modulo-2 addition;

¹We will be referring to the degree distribution selector located at the transmitter by DDS_T .

- 5) (*Modified intermediate bit sequence*) After calculating the value of each of the bits in \mathbf{b} , the same pilot bit sequence \mathbf{p} is again attached as in the initial step to the beginning of the intermediate bit sequence \mathbf{b} generated in the previous step in order to create $\mathbf{b}' = [\mathbf{p} \mathbf{b}]$;
- 6) (*Codeword bit calculation*) Determine the value of the encoded bit $c_i \in \mathbf{c}$, $i = 1, \dots, K' R_\iota^{-1}$ by calculating the values of $c_1 = b'_1$ and of $c_i = b'_i \oplus c_{i-1}$ for $i = 2, \dots, K' R_\iota^{-1}$, where $b'_i \in \mathbf{b}'$ and \oplus represents the modulo-2 addition operation. The pilot bits in \mathbf{c} correspond to the bits $c_i \in \mathbf{c}$ with $i = 1, \dots, K_p$.

For clarity, we have also provided a pictorial representation of this rateless encoding process in Figure 3. It can also be readily demonstrated that the number of pilot symbols required according to the predetermined pilot overhead δ_1^p is given by $K_p = (K \delta_1^p) / (R_\iota - \delta_1^p)$. The achievable throughput, T_{eff} , measured in bits/second/Hz, which also takes into consideration the power allocated to the pilot symbols, is then given by $T_{\text{eff}} = R_\iota - \delta_1^p$. It also follows that the proposed PSAR codes can realize any code having $R_\iota > \delta_1^p$. This implies that whilst other rateless codes such as LT codes [4] are capable of generating codes having an arbitrary rate, PSAR codes can only generate codes having rates that are higher than the fraction of pilots δ_1^p in the code. At first glance this might appear to be a limitation, however we note that δ_1^p is selected according to the highest expected fading rate, and hence for slow-fading channels PSAR codes can practically realize codes having any rate. Moreover, it is more power-efficient for the transmitter to opt for no transmission when the channel's SNR is very low, instead of transmitting at a very low code-rate.

We deliberately opted for describing the encoding process of PSAR codes in a similar manner to that used in [4], in order to make it easier to point out the similarities as well as the differences for the encoding technique used by proposed codes and that of the Luby Transform (LT) codes of [4]. We also wish to point out the fact that most rateless codes do have a fixed-rate counterpart; in fact, the proposed PSAR codes can be viewed as instances of rateless repeat accumulate (RA) codes [12], that are however interspersing pilot bits with the actual encoded bits.

The third step of the rateless encoding procedure described above, ensures that the variable or information node distribution, $v_\iota(x)$, is regular, as defined by $v_\iota(x) := x^{d_v-1}$, where d_v denotes the variable node degree, i.e. the number of times each input bit $a'_i \in \mathbf{a}'$ has been selected. The distribution $v_\iota(x)$ is

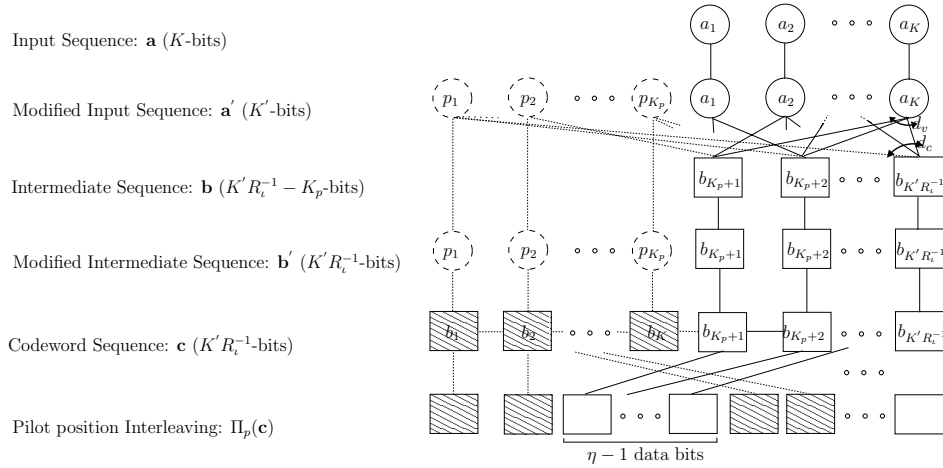


Fig. 3. The rateless encoder.

calculated by the DDS_T block of Figure 2 by using a similar technique to that used to determine $\delta_i(x)$. A more detailed explanation of the procedure used by the DDS will be offered in Section VI.

B. Pilot-Bit Interleaving and Space-Time Block Coding

As shown in Figure 3, the codeword \mathbf{c} is then interleaved by the pilot position interleaver Π_p , which will position a pair of pilots every $(\eta - 1)$ data bits, where η denotes the pilot spacing. This process is similar to that described in [13], which represents the effective sampling of the channel's complex-valued envelope at a rate that is higher than the Nyquist rate and thus allowing the receiver to extract the channel attenuation as well as phase rotation estimates for each bit. The data bits are separated by means of a pair of pilot bits (instead of a single pilot), since the channels between the two transmit and two receive antennas have to be estimated. The interleaved codeword $\pi_p(\mathbf{c})$ is then modulated and re-encoded using the rate-one STBC specified by the transmission matrix \mathbf{G}_2 [11]. In this regard, let $\mathbf{s} = [s_1 \ s_2]^T$, where s_1 and s_2 represent two consecutive bits of the modulated sequence $\pi_p(\mathbf{c})$ of Figure 3 respectively. Correspondingly, the space-time codeword \mathbf{C} is represented by:

$$\mathbf{C} = \begin{bmatrix} s_1 & s_2 \\ -s_2^* & s_1^* \end{bmatrix}, \quad (2)$$

where $(\cdot)^*$ is the complex-conjugate operator.

C. Inner Closed-Loop System: MIMO Transmit Eigen-beamforming

The inner closed-loop system, depicted in Figure 4, consists of a single-user MIMO system employing two transmit and two receive antennas. Let the channel impulse responses (CIRs) be stored in the (2×2) -element channel matrix \mathbf{H} containing four elements corresponding to an independent and identically-distributed (i.i.d) complex-valued Gaussian distributed random variables having zero mean and unity variance. The transmit eigen-beamforming scheme can be decomposed in three main components [3], consisting of the input-shaping matrix \mathbf{V}_C representing the eigenvectors of the covariance matrix of the encoded codeword \mathbf{C} , the beamforming matrix \mathbf{V}_H and the power allocation vector

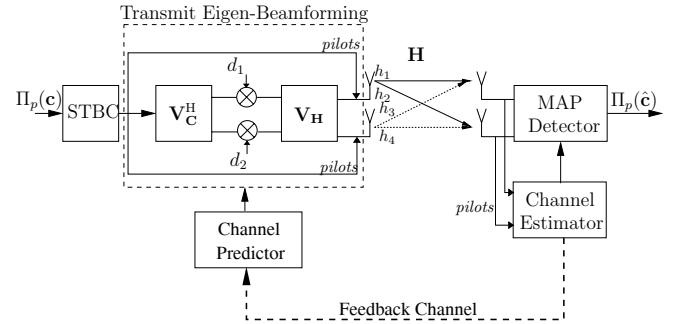


Fig. 4. The inner closed-loop system, in which the Alamouti space-time codeword is first spatially de-correlated and then decoupled into spatially orthogonal modes matching the eigen-directions of the MIMO channel.

$\mathbf{d} = [d_1 \ d_2]$. These three matrices are formulated by $\text{cov}(\mathbf{C}) = \mathcal{E}(\mathbf{C}\mathbf{C}^H) = \mathbf{V}_C \mathbf{\Lambda}_C \mathbf{V}_C^H$, where $(\cdot)^H$ denotes the Hermitian transpose operator. The matrix $\mathbf{\Lambda}_C = \text{diag}[\lambda_{C_1} \ \lambda_{C_2}]$, where $\text{diag}[\cdot]$ has elements in the leading diagonal and λ_{C_i} with $i = [1, 2]$ correspond to the eigenvalues of \mathbf{C} . The task of the input-shaping matrix \mathbf{V}_C , also shown in Figure 4, is to spatially de-correlate the input signal so as to disperse the input energy in the most effective way across the Alamouti space-time codeword.

On the other hand, the beamforming matrix \mathbf{V}_H is the right-hand side (RHS) singular matrix of the MIMO channel matrix \mathbf{H} , hence we have $\mathbf{H} = \mathbf{U}_H \mathbf{\Lambda}_H^{\frac{1}{2}} \mathbf{V}_H^H$, where \mathbf{U}_H represents the unitary, left-hand side singular matrix of \mathbf{H} , $\mathbf{\Lambda}_H^{\frac{1}{2}} = \text{diag}[\sqrt{\lambda_{H_1}} \ \sqrt{\lambda_{H_2}}]$ and λ_{H_i} with $i = [1, 2]$ corresponds to the eigenvalues of the $\mathbf{H}^H \mathbf{H}$. The beamforming matrix \mathbf{V}_H decouples the input signal into spatially orthogonal modes in order to match the eigen-directions of the MIMO channel.

At each transmission instant, a column of the space-time codeword \mathbf{C} seen in (2), will be linearly transformed by the transmit eigen-beamforming matrix \mathbf{P} before transmission, where \mathbf{P} is formulated by $\mathbf{P} = \mathbf{V}_C^H \mathbf{\Lambda}_P \mathbf{V}_H$, having $\mathbf{\Lambda}_P = \text{diag}[\mathbf{d}]$. The total transmission power at every instant is normalized to unity and controlled by the power allocation vector \mathbf{d} . Based on the ergodic capacity-optimization criterion, the power is allocated according to the classic waterfilling algorithm. The power allocated for each layer, P_i , is first

calculated based on [3]

$$P_i = \left(\mu - \frac{N_0}{\lambda_{\mathbf{H}_i}} \right) \mathbf{1} \left\{ \left(\mu - \frac{N_0}{\lambda_{\mathbf{H}_i}} \right) > 0 \right\}, \text{ for } i = [1, 2], \quad (3)$$

where $\mathbf{1}\{\cdot\}$ denotes the indicator function returning a value of one, if the argument is true, and zero otherwise, and μ denotes what is referred to as the water surface level [14]. Furthermore, P_i must satisfy the total power constraint of $\sum_{i=1}^2 P_i = 1$. After calculating the value of P_i , the value of the corresponding power gain $d_i \in \mathbf{d}$, seen in Figure 4, is given by $d_i = \sqrt{P_i/\lambda_{C_i}}$, where λ_{C_i} is the corresponding eigenvalue element residing on the leading diagonal. Furthermore, we note that as illustrated in Figures 2 and 4, the space-time codeword corresponding to a pair of pilot bits will bypass the transmit eigen-beamforming stage.

D. Receiver

We denote the pilot bits received at the first and second antenna on the first and second time-slot by $y_{1,1}$, $y_{1,2}$, $y_{2,1}$ and $y_{2,2}$, respectively. The four pilot bits, periodically occurring every $(\eta - 1)$ data bits, are then passed to the channel estimator (please refer to Figures 2 and 4), used for generating the corresponding MIMO channel matrix $\hat{\mathbf{H}}$ having elements of \hat{h}_1 , \hat{h}_2 , \hat{h}_3 and \hat{h}_4 formulated by $\hat{h}_1 = \frac{-\sqrt{2}}{2}(y_{1,1} + y_{1,2})$, $\hat{h}_2 = \frac{-\sqrt{2}}{2}(y_{2,1} + y_{2,2})$, $\hat{h}_3 = \frac{\sqrt{2}}{2}(y_{1,1} - y_{1,2})$, $\hat{h}_4 = \frac{\sqrt{2}}{2}(y_{2,1} - y_{2,2})$, where the scaling factor $\sqrt{2}$ results from the normalization of the transmit power to unity, as alluded to in Section III-C. The channel estimates are then up-sampled and interpolated by means of a low-pass interpolator [15]. Armed with this MIMO channel estimate, the received signal is then detected using a soft-input soft-output (SISO) maximum a-posteriori probability (MAP) detector. The detected signal is then de-interleaved using the pilot position interleaver Π_p described in Section III-B, and then passed to the rateless decoder, which estimates the original information bit sequence, i.e. \hat{a} .²

E. Feedback Link

The MIMO channel estimate $\hat{\mathbf{H}}$ is quantized according to a predetermined finite set of Z quantization levels. The selected quantization level I_z , where $z = 1, \dots, Z$, is then transmitted by the MS back to the BS over the feedback channel. The BS performs the inverse-quantization by reconstructing $\hat{\mathbf{H}}$ using the index value I_z received on the feedback channel. Based on the previous observations of the channel at time instant $t_0, t_0 - \eta, \dots, t_0 - k\eta$, where t_0 denotes the current time instant, the long-term channel predictor (LTCP) predicts the future CIR taps several instances into the future [16]. As further CSI information is received, the LTCP replaces the previously predicted values with the actual received CSI values.

²It is also implicitly assumed that there is another subsidiary DDS located at the receiver, namely DDS_R (not shown in the figures), that calculates the distributions $\delta_i(x)$ and $v_i(x)$ based on the estimated CSIR and then passes these distributions to the rateless decoder to be described in Section VI.

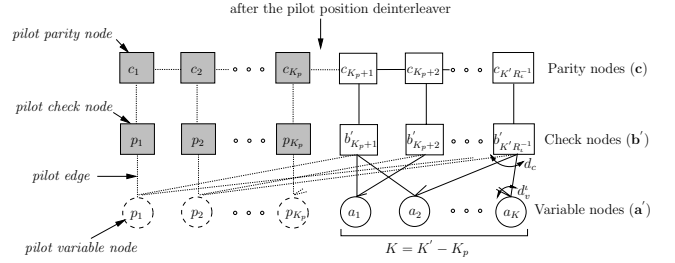


Fig. 5. A tripartite graph representation of a specific pilot symbol assisted rateless code for the transmission instance l .

IV. GRAPH-BASED ANALYSIS OF PILOT SYMBOL ASSISTED RATELESS CODES

The pilot symbols in PSAR codes are embedded in the actual codeword in such a way that they can be used not only for deriving the channel's amplitude and phase, but also for supporting the convergence of the iterative rateless decoder as well as for enhancing its performance. A Tanner graph representation of a PSAR code is provided in Figure 5, which shows an unbalanced tripartite graph G consisting of the finite set of vertices V and the finite set of edges E . The vertices set V can be further divided into three disjoint sets representing the variable nodes, the check nodes and the parity nodes. Following the notation introduced in Section III-A, the variable (information) nodes would then correspond to \mathbf{a}' , the check (intermediate) nodes are represented by \mathbf{b}' whilst the parity nodes relate to the PSAR-encoded codeword bits \mathbf{c} . Given the graph G , $G(v)$ will then denote the set of vertices adjacent to the vertex $v \in V$. The degrees d_v and $d_c \in \mathbf{d}'$ correspond to the discrete values assumed by the variable node distribution $v_i(x)$ and the check node distribution $\delta_i(x)$, respectively. The actual design of these two distributions will be the subject of Section VI.

PSAR codes also possess what we refer to as pilot nodes and pilot edges. Formally, we have the *pilot variable nodes*, $p_i \in \mathbf{a}'$, where $i = 1, \dots, K_p$, of degree d_v , having a known value, which hence do not carry any information, as opposed to the remaining variable nodes. Then, the *pilot check nodes*, $p_i \in \mathbf{b}'$, where $i = 1, \dots, K_p$, are the degree-one check nodes connected by a single edge to the pilot variable nodes. The output of the accumulator contains the *pilot parity nodes*, $c_i \in \mathbf{c}$, where $i = 1, \dots, K_p$. The pilot parity nodes are further interleaved by means of the pilot position interleaver, Π_p , which positions pairs of pilot parity nodes every other $(\eta - 1)$ parity nodes apart. The channel's complex-valued envelope is estimated by means of these pilot parity nodes. Finally, we also have the *pilot edges*, seen in Figure 5, consisting of the edges emerging from the pilot variable nodes and those joining the pilot check nodes to the pilot parity nodes. There are a total of $K_p d_v$ pilot edges between the variable and check nodes, and a further $2K_p$ pilot edges between the check and the parity nodes. It is also important to note from Figure 5, that in order to ensure the initialization of the iterative decoding convergence, the pilot edges sprouting from the K_p pilot variable nodes are not only associated with the pilot check nodes, but are also involved in other parity-check equations containing higher-degree check nodes. The messages passed over the pilot edges are perfectly

known, since they originate from nodes having predetermined values.

V. EXIT CHART FUNCTIONS OF PILOT SYMBOL ASSISTED RATELESS CODES

The rateless decoder of PSAR codes - which is represented by the tripartite graph of Figure 5 - is effectively constituted by the serial concatenation of two decoders separated by a uniform random interleaver. The inner decoder is the amalgam of a memory-one trellis decoder used for the accumulator (ACC) and of a check node decoder (CND), whilst the outer decoder is a variable node decoder (VND). The convergence behavior of this decoding process can then be analyzed in a similar manner to that used for other iterative decoding processes by means of observing the evolution of the input and output mutual information exchange between the inner and outer decoders in consecutive iterations, which is diagrammatically represented using the semi-analytical tool of EXIT charts [17]. There exists a direct one-to-one mapping between the two EXIT curves $I_{D\&A\&C}$ and I_{VND} as well as the corresponding check and variable node distributions, $\delta_l(x)$ and $v_l(x)$. Given the pair of distributions $v_l(x)$ and $\delta_l(x)$, we can then proceed to determine the corresponding EXIT curves representing the two EXIT functions of both the inner and outer decoders.

The combined EXIT function $I_{E,D\&A\&C}(\cdot)$ of the detector, accumulator and CND can be approximated as in [17] by:

$$I_{E,D\&A\&C}(I_A, I_E, \mathbf{d}^t, \psi_{\text{avg}}) \approx \sum_{\forall d_c \in \mathbf{d}^t} \Delta_{d_c}^t \left[1 - J \left(\sqrt{(d_c - 1) \cdot [J^{-1}(1 - I_A)]^2 + [J^{-1}(1 - I_E)]^2} \right) \right], \quad (4)$$

where the function $J(\cdot)$ denotes the mutual information and $I_A := I_{A,CND} = I_{A,D\&A\&C}$ represents the *a-priori* information input of the CND. The extrinsic information accumulator output is then defined by $I_E := I_{E,ACC} [I_{A,ACC}(I_{A,CND}, \mathbf{d}^t), I_{E,D}(\psi_{\text{avg}})]$, where $I_{A,ACC}$ denotes the *a-priori* accumulator information input and $I_{E,D}$ represents the extrinsic information detector output. The parameter $\Delta_{d_c}^t$ in (4) corresponds to the specific fraction of edges emanating from the intermediate bits (or check nodes) of degree $d_c \in \mathbf{d}^t$ and is given by

$$\Delta_{d_c}^t = \delta_{d_c} \cdot \frac{d_c}{d_{c,\text{avg}}}, \quad (5)$$

and the average check node degree $d_{c,\text{avg}}$ is defined by $d_{c,\text{avg}} := \sum_{\forall d_c \in \mathbf{d}^t} \delta_{d_c} \cdot d_c$. Then, by substituting $\delta_1 = \delta_1^p + \delta_1^{\bar{p}}$ into (5) for $d_c = 1$, the fraction of edges attributed to the degree-one pilot nodes as well as to the non-pilot check nodes is given by $\Delta_{d_1}^t = (\delta_1^p + \delta_1^{\bar{p}}) / (d_{c,\text{avg}})$.

For the particular case of the proposed PSAR codes (and thus in contrast to [17]), the inner decoder's EXIT function $I_{E,D\&A\&C}(\cdot)$ can be analyzed in terms of three separate components as in (6) (cf. p. 7). The first component of (6) represented by the function $I_{E,D\&A\&C}^1(\cdot)$ is determined by using (4) and by substituting $d_c \in \mathbf{d}^t$ for all the check nodes that are higher than one. It may be readily shown that the second and third constituent functions of (6) are then

approximated by

$$\begin{aligned} I_{E,D\&A\&C}^2(\cdot) &\approx \frac{\delta_1^{\bar{p}}}{d_{c,\text{avg}}} \left[1 - J \left(\sqrt{[J^{-1}(1 - I_E)]^2} \right) \right] \\ &= \frac{\delta_1^{\bar{p}}}{d_{c,\text{avg}}} I_E, \end{aligned} \quad (7)$$

whilst $I_{E,D\&A\&C}^3(\cdot)$ is determined by the multivariable limit formulated by (8). In (8), we are seeking the limit as $(I_A, \psi_{\text{avg}}) \rightarrow (1, \infty)$ since the fraction δ_1^p corresponds to pilot check nodes (please refer to Figure 5), which receive perfect messages from both the pilot parity nodes as well as from the pilot variable nodes. Subsequently, we can substitute (6), (7) and (8) into (4), yielding (9).³

Given a variable node distribution v_l , the outer decoder's EXIT function representing the extrinsic information output of the VND can be formulated in a similar manner to that of a non-systematic RA code [17], namely as:

$$I_{E,VND}(I_{A,VND}, d_v) = J \left[\sqrt{(d_v - 1) J^{-1}(I_{A,VND})} \right], \quad (10)$$

where $I_{E,VND}(I_{A,VND}, d_v)$ represents the extrinsic information output of the VND as a function of the its *a-priori* information input $I_{A,VND}$ and its variable node degree d_v .

VI. EXIT CHART BASED OPTIMIZATION FOR PILOT SYMBOL ASSISTED RATELESS CODES

This section details the technique employed by the degree distribution selectors in order to determine the specific check and variable node distribution, $\delta_l(x)$ and $v_l(x)$ that maximizes the achievable code-rate. This optimization problem is tackled by the following linear programming approach, with the primal problem formulated by

$$\max \sum_{\forall d_c \in \mathbf{d}^t} \frac{d_c}{\Delta_{d_c}^t} \quad (11)$$

subject to the *equality constraint* of

$$\sum_{\forall d_c \in \mathbf{d}^t} \Delta_{d_c}^t = 1 \quad (12)$$

and to the *inequality constraints* given by

$$I_{E,D\&A\&C}(\mathcal{I}, \mathbf{d}^t, \psi_{\text{avg}}) > I_{A,VND}(\mathcal{I}, d_v) + \varsigma, \quad (13)$$

and

$$\Delta_{d_c}^t |_{\forall d_c \in \mathbf{d}^t} > 0, \quad (14)$$

where (12) and (14) ensures that the resultant $\Delta_{d_c}^t$ values are both valid and non-negative. The parameter \mathcal{I} represents the discrete set of gradually increasing values in the interval $[0, 1]$ over which the functions $I_{E,D\&A\&C}(\cdot)$ and $I_{A,VND}(\cdot) = I_{E,VND}^{-1}(\cdot)$ (please refer to (9) and (10)) are calculated, whilst ς assumes values across \mathcal{I} , which determines the area of the tunnel between the two EXIT curves. This area has a direct relationship to the number of iterations required in order to reach the (1,1) point of the EXIT chart. Optimizing the objective function of (11) subject to the above-mentioned constraints, will determine the feasible set of

³The initialization of convergence for this rateless iterative decoding process is guaranteed by the term $\frac{1}{d_{c,\text{avg}}} (\delta_1^p + \delta_1^{\bar{p}} I_E)$ in (9).

$$I_{E,D\&A\&C}(\cdot) \approx I_{E,D\&A\&C}^1(I_A, I_E, \psi_{\text{avg}}, \forall d_i \in \mathbf{d}^l | i > 1) + I_{E,D\&A\&C}^2(I_A, I_E, \psi_{\text{avg}}, \forall d_1 \in \mathbf{d}^l | \delta_1 = \delta_1^{\bar{p}}) + I_{E,D\&A\&C}^3(\forall d_1 \in \mathbf{d}^l | \delta_1 = \delta_1^p). \quad (6)$$

$$I_{E,D\&A\&C}^3(\cdot) \approx \lim_{(I_A, \psi_{\text{avg}}) \rightarrow (1, \infty)} \frac{\delta_1^p}{d_{c,\text{avg}}} [1 - J([J^{-1}(1 - I_E)])] = \frac{\delta_1^p}{d_{c,\text{avg}}}. \quad (8)$$

$$I_{E,D\&A\&C}(\cdot) \approx \frac{1}{d_{c,\text{avg}}} (\delta_1^p + \delta_1^{\bar{p}} I_E) + \sum_{\forall d_c \in \mathbf{d}^l \setminus d_1} \Delta_{d_c}^l [1 - J(\sqrt{(d_c - 1) \cdot [J^{-1}(1 - I_A)]^2 + [J^{-1}(1 - I_E)]^2})]. \quad (9)$$

candidate solutions having values of $\Delta_{d_c}^l$ (and consequently δ_{d_c}) corresponding to the specific check node degrees $d_c \in \mathbf{d}^l$ that substantiate that distribution $\delta_i(x)$, which maximizes the design rate, for a predefined d_v value.

Nevertheless, we remark that the constraints represented in (12), (13) and (14) on their own are not sufficient to guarantee that the resultant PSAR code will provide a δ_1^p -fraction of pilot bits. For this particular reason, a stricter constraint than that of (14) must be introduced for the specific fraction of edges $\Delta_{d_1}^l$ terminating in degree-one check nodes, which must also obey $\Delta_{d_1}^l \geq \delta_1^p/d_{c,\text{avg}}$. The difficulty in satisfying the latter constraint arises from the dependence of $\Delta_{d_1}^l$ on the average check node degree $d_{c,\text{avg}}$, where the latter is again dependent on the value of $d_c \in \mathbf{d}^l$ as well as on the value of δ_{d_c} , both of which constitute part of the set of solutions for the optimization problem considered. This problem is circumvented by utilizing a search algorithm, similar to a binary search algorithm, which progressively finds better estimates of the required $\Delta_{d_1}^l$ value that results in the required δ_1^p -fraction of pilot bits. We note that a conventional binary search algorithm cannot be directly applied in this scenario due to the continuous nature of $\Delta_{d_1}^l$, which prevents its representation in a sorted array.

The first step of the PSAR code design technique was that of solving the optimization problem of (11) satisfying the constraints of (12), (13) and (14), and temporarily setting δ_1^p to zero. This initial step is carried out in order to estimate the number of degree one check nodes that are available. The fraction of degree one nodes, δ_1 , is then calculated according to (5) and using the $\Delta_{d_1}^l$ value resulting from the first run of the linear program.

For the sake of further explaining the procedure used, we will denote the fraction of edges and nodes calculated after the i^{th} evaluation of the objective function of (11) by $\Delta_{d_1,i}^l$ and $\delta_{1,i}$, respectively. Following this, if the resultant initial value $\delta_{1,1}$ is smaller than the target value δ_1^p , the linear program is run again by introducing a fourth inequality constraint given by $\Delta_{d_1}^l > 2\Delta_{d_1,1}^l$. In doing so, the value $\Delta_{d_1,1}^l$ is set to be the (temporarily) lowest value of the search interval $\Delta_{d_1}^l$. After the second iteration, which provides the solution for both $\Delta_{d_1,2}^l$ and for the corresponding fraction $\delta_{1,2}$, a comparison is made again between $\delta_{1,2}$ and the target fraction of pilots. If the value of $\delta_{1,2}$ is found to be larger than δ_1^p , the value of $\Delta_{d_1,2}^l$ is set to be the (temporarily) highest value of the search interval. The search may then continue by solving the objective function of (11) for the third time, with the additional fourth

constraint of $\Delta_{d_1}^l > (\Delta_{d_1,2}^l - \Delta_{d_1,1}^l)/2$. On the other hand, if the calculated value $\delta_{1,2}$ is again smaller than the target value, the value $\Delta_{d_1,2}^l$ becomes the new lowest value of our search interval and the additional fourth constraint is twice this lowest value; i.e. $\Delta_{d_1}^l > 2\Delta_{d_1,2}^l$. Following this, every further run of the linear program will enable use to narrow our search interval by a factor of two, until the target value is found.

The procedure used is shown summarized in Algorithm 1. It can be observed that the modified binary search algorithm is not applied in the case, when we have $\delta_{1,1} > \delta_1^p$. For a reasonable number of required pilots, this specific scenario will only occur when the channel SNR is very low. We initially also attempted to search for the target value in this specific scenario; i.e. by setting $\delta_{1,i}$ to correspond to the upper value of our search interval. However, the resultant code rate was found to be lower to that obtained without carrying out the search. This phenomenon can be explained by the fact that searching for a target value which is lower than the initial $\delta_{1,1}$ -fraction will unavoidably shift the combined inner decoder's EXIT curve downwards. Consequently, the linear program will then opt for a higher d_v value in order to bring the outer decoder EXIT curve down to a point that satisfies the constraint of (13). In doing the so, the resulting code rate will inevitably be lower, since R^l is inversely proportional to the variable node degree. Furthermore, from the point of view of the decoder, it is clearly understandable that the lower the value of the channel SNR is, the higher must be the δ_1 -fraction in the degree distribution in order to limit the propagation of flawed messages from the check nodes to a large number of variable nodes. Hence, we have purposely carried out our analysis by assuming that the δ_1 -fraction of degree one check nodes contains both pilots as well as non-pilot nodes.

Another benefit of the proposed system is that of fully exploiting the (inherent) flexibility of rateless codes, where the degree distributions are also calculated 'on-the-fly' by the degree distribution selectors. We also take a further step away from the commonly shared conception that EXIT charts are only suitable to design decoders. We further argue that successful decoding can only be guaranteed if and only if a suitable encoding strategy using a carefully designed pair of distributions, $\delta_i(x)$ and $v_i(x)$ is employed at the transmitter. In this way, the proposed generalized transmit preprocessing system serves as a successful example of joint transmitter and receiver design having a *pre-encoding stage*, whereby the degree distributions are calculated by the DDS_T, followed

Algorithm 1: The EXIT chart based optimization of PSAR codes

input : $d_v, \mathcal{I}, \varsigma, \delta_1^p, \psi_{\text{avg}}$
output: $\Delta_{d_c}^l, \mathbf{d}^l$

```

1 Initializations: target value  $\leftarrow \delta_1^p$ , (iteration)  $i \leftarrow 0$ 
2 while  $\delta_{1,i} < \text{target value}$  do
3      $i \leftarrow i + 1$ 
4     if  $i = 1$  then
5         Solve the optimization problem of (11) satisfying
           the constraints of (12), (13) and (14), and
           temporarily setting  $\delta_1^p$  to zero.
6          $\delta_{1,i} \leftarrow \delta_1$ ,  $\Delta_{d_{1,1}}^l \leftarrow \Delta_{d_1}^l$ . Set fourth constraint for
           iteration  $i = 2$ :  $\Delta_{d_1}^l > 2\Delta_{d_{1,1}}^l$ .
7     else
8         Solve the optimization problem of (11) subject to
           the constraints of (12), (13), (14) and the
           additional fourth constraint set in iteration  $i - 1$ .
9          $\delta_{1,i} \leftarrow \delta_1$ ,  $\Delta_{d_{1,i}}^l \leftarrow \Delta_{d_1}^l$ .
10        if  $\delta_{1,i} < \text{target value}$  then
11            Fourth constraint for iteration  $i + 1$ :
12             $\Delta_{d_1}^l > 2\Delta_{d_{1,i}}^l$ .
13        else if  $\delta_{1,i} > \text{target value}$  then
14            Fourth constraint for iteration  $i + 1$ :
15             $\Delta_{d_1}^l > 0.5(\Delta_{d_{1,i}}^l - \Delta_{d_{1,i-1}}^l)$ .
16        else
17            Target value has been reached. Return output
           parameters.
18    end
19 end
    
```

by a *pre-transmission stage*, where the codeword is linearly transformed by the transmit eigen-beamforming matrix in order to mitigate the detrimental effects of the channel.

VII. SIMULATION RESULTS

The results presented in this section were obtained using BPSK modulation, when transmitting over a correlated Rayleigh channel. The proposed rateless codes were decoded using the classic belief propagation (BP) algorithm, in a similar fashion to the decoding of low-density parity-check (LDPC) codes. The rateless decoder was limited to a maximum of $I_{\text{max}} = 200$ iterations. Three different mobile terminal's velocities were considered; a pedestrian speed of 3 mph, and vehicular speeds of 60 mph as well as of 100 mph. The data signaling rate and the carrier frequency were those from the Universal Mobile Telecommunication System (UMTS) standard, and were set to 15 kbps and 2 GHz, respectively.

Figure 6 illustrates the exhibited average throughput performance parameterized with the mobile terminal velocity, for the range of channel SNR values considered. It can be observed that by increasing the velocity from 3 mph to 100 mph, the throughput performance suffers a loss of approximately 0.1 bits/channel use in the high SNR region. The difference in the throughput performance between the 3 mph and 100 mph scenario in the low-to-medium channel SNR region was

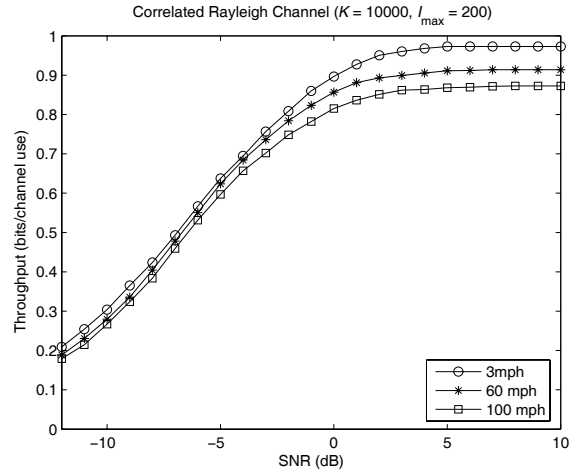


Fig. 6. A comparison of the achievable average throughput performance (measured in bits/channel use) versus the SNR (in dB) for transmission over an correlated Rayleigh channel using BPSK modulation. The number of information bits for the rateless code, K , was set to 10,000 bits and the maximum number of decoder iterations, I_{max} was fixed to 200 iterations. The mobile terminal's velocity was set to 3 mph, 60 mph and 100mph. The fraction of pilot bits, δ_1^p , was set to 0.05 (for the 3 mph and 60 mph scenario) and to 0.1 (for the 100 mph scenario).

about 0.5 dB. The effect of the maximum number of affordable decoder iterations on the achievable average throughput performance is then portrayed in Figure 7. Reducing I_{max} from 200 to 50 iterations results in an average throughput performance loss of approximately 0.05 bits/channel use in the high SNR region and a 1 dB away from the theoretical capacity curve in the low-SNR region.

Figures 8 and 9 illustrate our comparison of the achievable throughput performance as well as the rateless decoder's computational complexity for both the proposed PSAR code-aided, generalized MIMO transmit preprocessing scheme and for a benchmarker. The benchmarker is the same transmit preprocessing scheme, but instead of having a PSAR code, we use a rateless code dispensing with pilots (i.e. we set $\delta_1^p = 0$ at the encoding stage, which was previously described in Section III-A), but then insert the required number of pilots at the modulation stage. In this sense, we are comparing pilot symbol assisted (rateless) coding with that of pilot symbol assisted modulation in an attempt to verify which of the two techniques offers a better performance (in terms of achievable throughput as well as complexity) for the same amount of pilot overhead.

In order to make a fair comparison, the parameters K and I_{max} were fixed to 10,000 bits and 200 iterations, for both systems. The mobile terminal's velocity was set to 100 mph. The fraction of pilot bits δ_1^p was set to 0.1 for the PSAR code, whilst 10% pilots were inserted at the modulation stage for the benchmarker system. The rateless decoder's computational complexity for both systems was evaluated in terms of the number of message-passing updates per decoded bit, given by $I_{\text{avg}}|E|/K$, where I_{avg} represents the average number of iterations required for finding a legitimate codeword at a particular channel SNR value and $|E|$ represents the number of edges in the corresponding Tanner graph.

It can be observed from Figure 8 that there is no difference

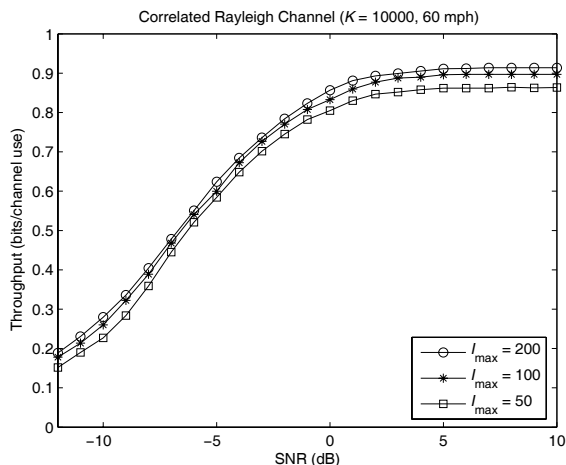


Fig. 7. A comparison of the achievable average throughput performance (measured in bits/channel use) versus the SNR (in dB) for transmission over an correlated Rayleigh channel using BPSK modulation. The number of information bits for the rateless code, K , was set to 10,000 bits and the maximum number of decoder iterations, I_{\max} was varied from 200 to 50 iterations. The mobile terminal's velocity was set to 60 mph and the fraction of pilot bits, δ_1^p , was set to 0.05.

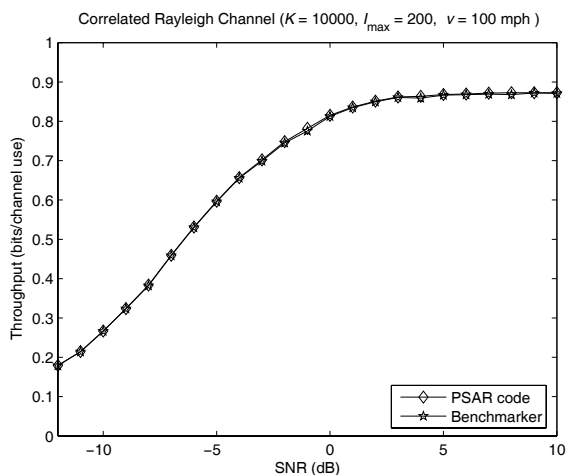


Fig. 8. A comparison of the achievable average throughput performance (measured in bits/channel use) by the PSAR code and the benchmarker scenario, versus the SNR (in dB), assuming transmission over an correlated Rayleigh channel using BPSK modulation. The benchmarker scenario consists of a rateless code, which is not aided with pilot symbols (i.e. set $\delta_1^p = 0$), and then followed by PSAM with a 10% pilot overhead. The number of information bits for both scenarios, K , was set to 10,000 bits and the maximum number of decoder iterations, I_{\max} was fixed to 200 iterations. The mobile terminal's velocity was set to 100 mph and the fraction of pilot bits for the PSAR code, δ_1^p , was set to 0.1.

in the throughput performance of the two systems. On the other hand, the proposed PSAR code-aided system offers a considerable reduction in the rateless decoder's computational complexity, as shown in Figure 9. It was found that the complexity reduction⁴ in this specific scenario is (on average) more than 30%. Similarly, we have observed a complexity reduction of 25%, when the mobile velocity was reduced

⁴The complexity reduction can also be explained in terms of the corresponding EXIT chart. The effect of the δ_1^p -fraction of pilot bits is that of widening the tunnel between the two decoder's EXIT curves, and thus reducing the decoder's computational complexity.

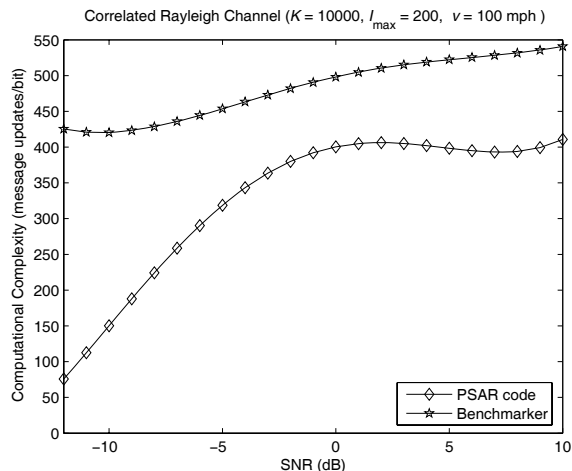


Fig. 9. A comparison of the rateless decoder's computational complexity (measured in message updates/bit) by the PSAR code and the benchmarker scenario, versus the SNR (in dB), assuming transmission over an correlated Rayleigh channel using BPSK modulation. The benchmarker scenario consists of a rateless code, which is not aided with pilot symbols (i.e. set $\delta_1^p = 0$), and then followed by PSAM with a 10% pilot overhead. The number of information bits for both scenarios, K , was set to 10,000 bits and the maximum number of decoder iterations, I_{\max} was fixed to 200 iterations. The mobile terminal's velocity was set to 100 mph and the fraction of pilot bits for the PSAR code, δ_1^p , was set to 0.1. It can be verified, that PSAR codes reduces the complexity by more than 30%, when compared with the corresponding benchmarker scenario.

from 100 mph to 60 mph. The δ_1^p -fraction of pilot bits was subsequently reduced from 0.1 to 0.05.

VIII. SUMMARY AND CONCLUDING REMARKS

In this paper, we have proposed a generalized framework for a MIMO transmit preprocessing aided closed-loop downlink system, in which both the channel coding components and the linear transmit precoder exploit the knowledge of the CSI. In order to achieve such an aim, we have embedded, for the first time, a rateless code in our transmit preprocessing scheme, in order to attain a near-capacity performance across a diverse range of channel SNRs. Furthermore, the proposed rateless codes that we have employed are capable of calculating (online) the required degree distributions before transmission based on the available CSIT. Hence the two CSI-assisted components at the transmitter; namely the rateless encoder and the linear MIMO precoder, may be interpreted as a generalized transmit preprocessing scheme, when compared to their previously proposed counterparts in the literature [3]. Using this scheme, we were able to attain a performance which is less than 1 dB away from the discrete-input continuous-output memoryless channel capacity over a diverse range of channel SNRs, rather than at a single SNR value, when transmitting over an uncorrelated Rayleigh channel using $K = 10,000$ bits.

We have also proposed a novel coding technique, hereby referred to as PSAR coding, where a predetermined fraction of pilot bits is appropriately interspersed, in a meticulous manner, along with the codeword bits at the channel coding stage, instead of inserting the pilots at the modulation stage, such as in classic PSAM. We note that our technique is generic, since it can be applied to any iterative decoding (ID)-aided

channel coding scheme. In fact, we recently discovered that a somewhat similar technique was employed in the context of regular LDPC codes [18]. In this paper, we have generalized the technique to also include non-systematic codes. We believe that the benefits of the proposed technique are more pronounced in non-systematic codes, whose ID process typically requires the employment of code doping for triggering their ID convergence. Subsequently, we have demonstrated that the PSAR code-aided MIMO transmit preprocessing scheme gleans more benefits from the inserted pilots than the classic PSAM technique, because the pilot bits are not only useful for sounding the channel at the receiver but also beneficial for significantly reducing the computational complexity of the rateless channel decoder. Our results suggest that more than a 30% reduction in the decoder's computational complexity can be attained when comparing the proposed system to an otherwise identical scheme using the classic PSAM technique. On the other hand, the inevitable energy and throughput loss imposed by the periodically inserted pilot symbols in the classic PSAM technique is only compensated by the capability of channel estimation.

REFERENCES

- [1] G. J. Foschini and M. J. Gans, "On limits of wireless communications in a fading environment when using multiple antennas," *Wireless Personal Commun.*, no. 6, pp. 315-335, 1998.
- [2] G. J. Foschini, "Layered space-time architecture for wireless communication in a fading environment when using multi-element antennas," *Bell System Technical J.*, pp. 41-59, Sept. 1996.
- [3] M. Vu and A. Paulraj, "MIMO wireless linear precoding," *IEEE Signal Process. Mag.*, vol. 24, pp. 86-105, Sept. 2007.
- [4] M. G. Luby, M. Mitzenmacher, M. A. Shokrollahi, and D. A. Spielman, "Efficient erasure correcting codes," *IEEE Trans. Inf. Theory*, vol. 47, pp. 569-584, Feb. 2001.
- [5] M. A. Shokrollahi, "Raptor codes," *IEEE Trans. Inf. Theory*, vol. 52, pp. 2551-2567, June 2006.
- [6] R. Palanki and J. S. Yedidia, "Rateless codes on noisy channels," in *Proc. IEEE International Symp. Inf. Theory*, Chicago, IL, USA, p. 37, June 2004.
- [7] J. Castura and Y. Mao, "Rateless coding over fading channels," *IEEE Commun. Lett.*, vol. 10, pp. 46-48, Jan. 2006.
- [8] U. Erez, G. W. Wornell, and M. D. Trott, "Rateless space-time coding," in *Proc. IEEE International Symp. Inf. Theory*, Adelaide, SA, pp. 1937-1941, Sept. 2005.
- [9] N. Bonello, R. Zhang, S. Chen, and L. Hanzo, "Reconfigurable rateless codes," in *Proc. IEEE 69th Veh. Technol. Conf.*, Barcelona, Spain, Apr. 2009.
- [10] O. Etesami and M. A. Shokrollahi, "Raptor codes on binary memoryless symmetric channels," *IEEE Trans. Inf. Theory*, vol. 52, pp. 2033-2051, May 2006.
- [11] S. M. Alamouti, "A simple transmit diversity technique for wireless communications," *IEEE J. Sel. Areas Commun.*, vol. 16, pp. 1451-1458, Oct. 1998.
- [12] H. Jin, A. Khandekar, and R. J. McEliece, "Irregular repeat-accumulate codes," in *Proc. 2nd International Symp. Turbo Codes Related Topics*, Brest, France, pp. 1-8, Sept. 2000.
- [13] J. K. Cavers, "An analysis of pilot symbol assisted modulation for Rayleigh faded channels," *IEEE Trans. Veh. Technol.*, vol. 40, pp. 686-693, Nov. 1991.
- [14] T. Cover and J. Thomas, *Elements of Information Theory*. New York: Wiley-Interscience, Aug. 1991.
- [15] *Programs for Digital Signal Processing*. New York: IEEE Press, 1979.
- [16] D. Yang, L. Wei, L.-L. Yang, and L. Hanzo, "Channel prediction and predictive vector quantization aided channel impulse response feedback for SDMA downlink preprocessing," in *Proc. IEEE 68th Veh. Technol. Conf.*, Calgary, Canada, 2008.
- [17] S. ten Brink and G. Kramer, "Design of repeat-accumulate codes for iterative detection and decoding," *IEEE Trans. Signal Process.*, vol. 51, pp. 2764-2772, Nov. 2003.
- [18] M.-K. Oh, H. M. Kwon, D.-J. Park, and Y. H. Lee, "Iterative channel estimation and LDPC decoding with encoded pilots," *IEEE Trans. Veh. Technol.*, vol. 57, pp. 273-285, Jan. 2008.



Nicholas Bonello received the B.Eng.(Hons) degree in Electrical Engineering from the University of Malta in 2004, the M.Sc. degree in Radio Frequency Communications Systems from University of Southampton, U.K., in 2006 and the Ph.D. degree in Wireless Communications from the University of Southampton, U.K., in 2009. His primary research interests include fixed-rate as well as rateless error correction techniques, signal processing and statistics.



Du Yang received the B.Eng. degree in communication engineering from the Beijing University of Posts and Telecommunications, China, in 2005, and the M.Sc. degree (with distinction) in Radio Frequency Communication Systems from the University of Southampton, U.K., in 2006. She is now a Ph.D. student at the University of Southampton. Her current research interests are in limited channel state information feedback, closed-loop MIMO transmission schemes, network MIMO and spatial modulation.



Sheng Chen (M'90-SM'97-F'08) obtained a BEng degree from the East China Petroleum Institute, Dongying, China, in 1982, and a PhD degree from the City University, London, in 1986, both in control engineering. In 2005, he was awarded DSc from the University of Southampton, Southampton, UK. Since 1999 he has been with the School of Electronics and Computer Science, the University of Southampton, UK. He previously held research and academic appointments at the Universities of Sheffield, Edinburgh and Portsmouth, all in UK.

Professor Chen's recent research works include adaptive signal processing, wireless communications, modelling and identification of nonlinear systems, neural network and machine learning, finite-precision digital controller design, evolutionary computation methods, and optimization. He has published over 280 research papers. In the database of the world's most highly cited researchers in various disciplines, compiled by Institute for Scientific Information (ISI) of the USA, Prof. Chen is on the list of the highly cited researchers in the engineering category, see <http://www.ISIHighlyCited.com>.



Lajos Hanzo FREng, FIEEE, FIET, DSc received his degree in electronics in 1976 and his doctorate in 1983. During his 31-year career in telecommunications he has held various research and academic posts in Hungary, Germany and the UK. Since 1986 he has been with the School of Electronics and Computer Science, University of Southampton, UK, where he holds the chair in telecommunications. He has co-authored 17 books on mobile radio communications totalling in excess of 10 000 pages, published in excess of 800 research papers, acted as

TPC Chair of IEEE conferences, presented keynote lectures and been awarded a number of distinctions. Currently he is directing an academic research team, working on a range of research projects in the field of wireless multimedia communications sponsored by industry, the Engineering and Physical Sciences Research Council (EPSRC) UK, the European IST Programme and the Mobile Virtual Centre of Excellence (VCE), UK. He is an enthusiastic supporter of industrial and academic liaison and he offers a range of industrial courses. He is also an IEEE Distinguished Lecturer as well as a Governor of both the IEEE ComSoc and the VTS. He is the acting Editor-in-Chief of the IEEE Press. For further information on research in progress and associated publications please refer to <http://www-mobile.ecs.soton.ac.uk>.